

**No signature of the saturation of giant dipole resonance width in medium-mass nuclei**

S. Mukhopadhyay<sup>1,2,\*</sup>, Pratap Roy<sup>1,2,†</sup>, Debasish Mondal,<sup>1</sup> Deepak Pandit,<sup>1,2</sup> Surajit Pal,<sup>1</sup> Balaram Dey,<sup>3</sup> Srijit Bhattacharya,<sup>4</sup> A. De,<sup>5</sup> T. K. Rana,<sup>1,2</sup> S. Kundu,<sup>1,2</sup> J. Sadhukhan,<sup>1,2</sup> C. Bhattacharya,<sup>1,2</sup> and S. R. Banerjee<sup>1</sup>


<sup>1</sup>Variable Energy Cyclotron Centre, 1/AF-Bidhannagar, Kolkata 700064, India

<sup>2</sup>Homi Bhabha National Institute, Training School Complex, Anushaktinagar, Mumbai 400094, India

<sup>3</sup>Department of Physics, Bankura University, Bankura 722155, India

<sup>4</sup>Department of Physics, Barasat Government College, Barasat, N 24 Pgs, Kolkata 700124, India

<sup>5</sup>Department of Physics, Raniganj Girls' College, Raniganj 713358, India

 (Received 26 February 2021; revised 1 August 2021; accepted 23 August 2021; published 13 September 2021)

An experimental study on the temperature ( $T$ ) dependence of giant dipole resonance (GDR) width was performed for the medium mass nucleus  $^{74}\text{Kr}$  in the range of  $T \approx 2\text{--}2.5$  MeV at an average angular momentum of  $26\hbar$  using the  $^{16}\text{O} + ^{58}\text{Ni}$  fusion reaction. The emitted high-energy  $\gamma$  rays and evaporated neutrons were measured in coincidence with low-energy discrete  $\gamma$ -ray multiplicities. The GDR parameters, nuclear level density parameter, and nuclear temperature were determined by the statistical model analysis of the high-energy  $\gamma$ -ray spectra as well as evaporated neutron spectra. The measured GDR width is found to increase monotonically with temperature, in contradiction with the recent observation of the width saturation in  $^{88}\text{Mo}$ . Comparisons of the measured data with predictions of the adiabatic thermal shape fluctuation model and its refined version, the critical temperature included fluctuation model, are presented and discussed.

DOI: [10.1103/PhysRevC.104.L031304](https://doi.org/10.1103/PhysRevC.104.L031304)

The  $\gamma$  decay of the giant dipole resonance (GDR) has been a promising tool to investigate the structure and dynamics of a hot and fast rotating nuclei. The isovector GDR mode, where protons oscillate against neutrons, can be built on any nuclear state and its overall characteristics depend only on the bulk properties of the system [1]. The evolution of nuclear shape and its fluctuations at extreme conditions of nuclear temperature ( $T$ ) and angular momentum ( $J$ ) are directly reflected in the GDR line shape, characterized by three important parameters: the strength ( $S_{\text{GDR}}$ ), the centroid energy ( $E_{\text{GDR}}$ ) and the width ( $\Gamma_{\text{GDR}}$ ). The strength parameter sets a useful benchmark for collectivity and its disappearance at very high temperature is predicted to be linked with the liquid-to-gas phase transition [2]. The centroid energy, that splits into various components for a deformed nucleus, provides valuable information on the nuclear shape. The most important parameter is the width of the resonance, which is related to the various damping mechanisms of the collective motion within the nuclear matter, and provides vital information on nuclear shear viscosity [3–5].

During the last four decades, one of the prime quests in this field has been how GDR width depends on  $T$  and  $J$  [6]. Although the intrinsic GDR width has a very weak dependence on temperature [7], the experimentally measured widths (except at low  $T$ ) increase with  $T$  and  $J$ . On the theoretical side, several models have been developed to explain the experimental observations. The most popular thermal shape

fluctuation model (TSFM) describes the increase in width as a consequence of  $J$ -driven nuclear deformation and  $T$ -driven shape fluctuations [8]. Alternatively, the microscopic phonon damping model (PDM) describes the broadening of the GDR width ( $T > 0$ ) via coupling of GDR excitation to the noncollective p-p and h-h configurations, that leads to the thermal damping of the GDR [9].

In recent years, extensive experimental studies at low temperature ( $T < 1.5$  MeV) over a wide mass region ( $A = 30\text{--}208$ ) [10–13] have established that the GDR width remains constant up to a certain critical temperature and increases thereafter. The observed nature has been successfully explained by both TSFM (after taking into account shell effects, pairing field fluctuations, and the GDR induced quadrupole moment) and PDM [11,14,15]. While for  $T < 2$  MeV we have a rather good understanding of the problem of the damping of the GDR, at higher temperatures the situation is more complex. In this temperature region ( $T > 2$  MeV), one of the long-standing issues is the saturation of the GDR width which was first seen in  $^{110}\text{Sn}$  [16] and subsequently around the  $A = 135$  mass region [17,18]. However, it was later pointed out by Kelly *et al.* [19] that at higher bombarding energies preequilibrium emission substantially lowers the average excitation energies and hence the estimated temperature. The detailed measurements by the authors (of Ref. [19]), together with a reanalysis of the previous experimental results, showed that the GDR width in Sn and nearby nuclei does not saturate and continues to increase up to temperature  $\approx 3.2$  MeV [19]. Further investigation carried out by Wieland *et al.*, [20] in  $^{132}\text{Ce}$ , minimizing the preequilibrium effect through the mass symmetric channel, also provided convincing evi-

\*supm@vecc.gov.in

†Present address: GSI Helmholtzzentrum für Schwerionenforschung, D-64291 Darmstadt, Germany.

dence against the saturation of GDR width at least up to 3.7 MeV. The TSFM could successfully explain the measured data (of Ref. [20]) after considering the evaporation width, and it was assumed that the issue had been settled. However, recently Ciemala *et al.* [21] performed an experiment in the medium mass nucleus  $^{88}\text{Mo}$  produced using the same experimental approach (i.e., mass-symmetric channel having negligible preequilibrium effect) and obtained almost similar GDR widths at temperatures of 2.0 and 3.1 MeV. Thus this experimental study claiming a saturation of GDR width has reopened the debate on this issue once again. The observed saturation effect in  $^{88}\text{Mo}$  was supposed to be due to two effects: an apparent weak dependence of the GDR width on temperature itself, and high rotational frequency driven deformations which were similar at both the temperatures [21]. Therefore, it is clear that more exclusive-studies disentangling the effect of  $T$  and  $J$  in the medium mass region ( $A < 100$ ) are essential to get a comprehensive picture of the correct description of the damping mechanism contributing to the GDR width. This is also crucial from the theoretical point of view because TSFM and PDM have contradictory predictions [6,21,22] on this particular issue.

In this Letter, the temperature dependence of the GDR width in the mass region  $A \approx 75$  at an average angular momentum of  $\approx 26\hbar$  is presented. The earlier experimental studies of the saturation effect were mostly performed at higher mass regions, and they mainly focused on the minimization of pre-equilibrium energy loss using mass-symmetric target-projectile combination. However, for  $^{88}\text{Mo}$  [21], although the same technique was followed, the spreads in temperatures were quite large (1.1 and 1.5 MeV). In the present work, we preferred an asymmetric target-projectile combination and restricted beam energy within 7–10 MeV/nucleon mainly to reduce the preequilibrium effect, which is appreciable at higher bombarding energies ( $> 10$  MeV/nucleon). The chosen beam energies were also crucial for avoiding any fission events which may further complicate the resultant  $\gamma$ -ray spectrum. The GDR and nuclear level density (NLD) parameters were determined precisely by the statistical model analysis of the high-energy  $\gamma$ -ray spectra as well as evaporated neutron spectra. The angular momentum of the compound nucleus was determined by measuring the low-energy  $\gamma$ -ray multiplicities. The present work shows that there is no indication of saturation of the GDR width in  $^{74}\text{Kr}$ , at least up to temperature  $T = 2.5$  MeV, even at higher angular frequencies. The present data also offer an opportunity to test the credibility of existing theoretical models in the  $A \approx 75$  mass region (where no systematic data are available so far).

The experiment was performed at the Variable Energy Cyclotron Centre (VECC), Kolkata, using accelerated heavy ion beams from the K130 Cyclotron. A self-supporting  $^{58}\text{Ni}$  target (99.48% purity) of thickness  $\approx 1$  mg/cm<sup>2</sup> was bombarded with beams of  $^{16}\text{O}$ . Three different beam energies of 116, 140, and 160 MeV were used to form the compound nucleus  $^{74}\text{Kr}$  at the initial excitation energies of 88, 107, and 123 MeV, respectively. A part of the LAMBDA high-energy photon spectrometer [23] (49 large BaF<sub>2</sub> detectors arranged in  $7 \times 7$  matrix) was used to measure the high-energy  $\gamma$  rays at  $90^\circ$  with respect to the beam axis. The detector array was

positioned at a distance of 50 cm from the target. Along with the LAMBDA spectrometer, a 50-element low energy  $\gamma$ -multiplicity filter array [24] was used (in coincidence with the high-energy  $\gamma$  rays) to estimate the angular momentum populated in the compound nucleus in an event-by-event mode and also to get a fast start trigger for time-of-flight (TOF) measurements. The filter array was split into two blocks of 25 detectors each and were placed on top and bottom of a specially designed scattering chamber at a distance of 5 cm from the target in a staggered castle type geometry. The data were recorded only when at least one detector of the LAMBDA array above a threshold of  $\approx 4$  MeV fired in coincidence with both the top and bottom multiplicity filters. In this trigger condition slightly higher angular momentum events are selected, thereby suppressing the nonfusion events which occur at low  $J$ . Special care was taken to suppress the background events, especially the cosmic backgrounds. The cyclotron rf time spectrum was recorded with respect to the multiplicity filter to minimize the random coincidences. The LAMBDA spectrometer was surrounded by a 10-cm-thick passive lead shield to block the  $\gamma$ -ray background. The cosmic muons were rejected by using their hit pattern in the highly granular LAMBDA array. In the offline analysis, angular-momentum-gated high-energy  $\gamma$ -ray spectra were reconstructed by the cluster summing technique [23]. The TOF technique was used to discriminate the neutrons from the high-energy  $\gamma$ -rays. The pulse shape discrimination (PSD) technique was adopted to reject the pile-up events in the individual detector elements by measuring the charge deposition over two integrating time intervals (30 ns and  $2\ \mu\text{s}$ ) [23].

The neutron energy spectra were measured using two liquid-scintillator-based neutron detectors (BC501A, 5 in. diameter and 5 in. long). The neutron detectors were placed at  $45^\circ$  and  $150^\circ$  with respect to the beam direction and at a distance of 200 cm from the target. Data were recorded in coincidence with a low energy  $\gamma$ -multiplicity filter array [24] in order to get the start trigger for TOF measurements and to estimate populated angular momentum in an event-by-event mode. The detector configuration and trigger condition of the multiplicity filter array were same as described earlier for high-energy  $\gamma$ -ray measurements. To convert the neutron TOF spectra to neutron energy, the prompt  $\gamma$  peak in the TOF spectrum was used as the time reference. The energy-dependent detection efficiencies of the neutron detectors were obtained using the Monte Carlo code NEFF [25]. The detector efficiency at low energies (1–10 MeV) was also measured experimentally using a standard  $^{252}\text{Cf}$  neutron source and was found to be in good agreement with the NEFF calculation [26]. The beam dump was kept at a distance of  $\approx 3$  m from the target position and was heavily shielded with several layers of lead and paraffin to minimize the contribution of background neutrons coming from the beam dump. The  $\gamma$ -ray background in the neutron energy spectra was removed by using both the pulse shape discrimination (PSD) and time of flight (TOF) methods. The background contribution coming from the scattered neutrons (from the surrounding materials) was estimated by putting a “shadow bar” consisting of 40-cm-thick high-density plastic (HDP) and 6-cm Pb blocks placed in between the target and the detectors. This essentially blocks

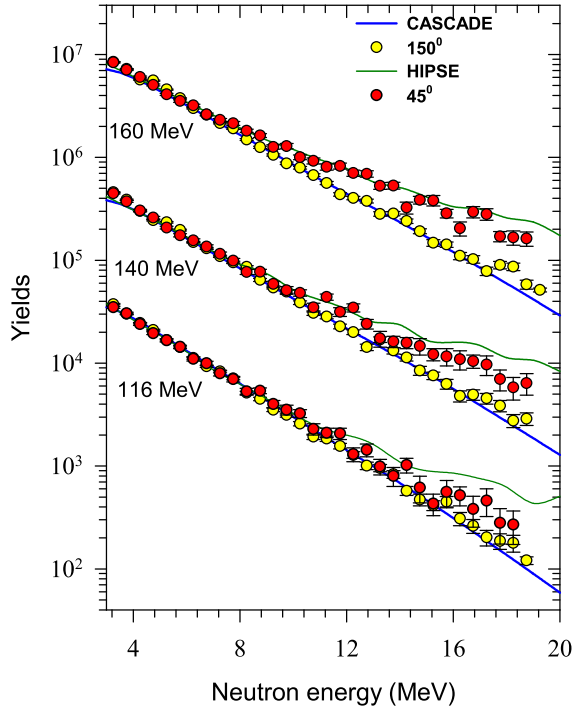


FIG. 1. Plot of angular momentum gated ( $(J) \approx 26\hbar$ ) neutron spectra, measured at backward (yellow circle) and forward angles (red circle) along with statistical model CASCADE calculation (solid blue line) and HIPSE calculation (thin green line). The spectra at different energies are scaled for better visualization.

the neutrons coming directly from the target and allows only the scattered neutrons in the detector. The contribution of scattered neutrons measured in this way was subtracted (with proper normalization) from the TOF data. The low-energy  $\gamma$ -ray multiplicity distribution, measured in coincidence with the neutron, was converted to angular momentum space with the help of a method discussed later. It should be emphasized here that a narrow angular momentum window corresponding to an average angular momentum of  $26\hbar$  was used for the generation of all the neutron as well as high-energy  $\gamma$ -ray spectra presented in this work, which ensures the study of the  $T$  dependence of the GDR parameters exclusively.

The background-corrected neutron spectra in the compound nucleus (CN) frame are shown in Fig. 1 for all the bombarding energies. The neutron spectra measured at the forward and backward angles were compared (Fig. 1) to look for any possible signature of preequilibrium emissions, which is expected to appear as an additional high-energy shoulder in the energy spectra of neutron at forward angle. The presence of such contribution is crucial since it signifies that the fusion is not complete and the system is not produced at the expected values of mass, spin, and excitation energy. In the measured spectra at forward angle, mild high-energy tails are visible. This suggests that the contribution of the preequilibrium emissions is small in the present study. This is in accordance with the experimental systematic available in the literatures [27,28] where such contribution was found to be within 5–7% for the present bombarding energy range.

The backward angle spectra agree nicely with the statistical model prediction (discussed later) as shown by the blue line in Fig. 1. This suggests that the back-angle spectra are mostly determined by the compound nuclear (equilibrated) emission, and hence they are used in the statistical model analysis for the extraction of the nuclear level density parameter.

The knowledge of average loss in excitation energy ( $E_{\text{Loss}}$ ) due to preequilibrium effect is important before doing statistical model analysis of the measured spectra. In this work  $E_{\text{Loss}}$  was estimated using the computer code HIPSE [29]. The  $E_{\text{Loss}}$  values obtained from HIPSE calculation (considering preequilibrium particle spectra of  $\alpha$ 's, protons, and neutrons and their corresponding multiplicities) are 4.3, 5.5, and 7.0 MeV for beam energies 116, 140, and 160 MeV, respectively. The estimated values are in reasonable agreement with the available experimental systematic [27,28]. The high-energy tails in the forward-angle neutron spectra shown in Fig. 1 are also well reproduced by the corresponding predictions of the HIPSE model considering both evaporation as well as preequilibrium processes. We mention here that the statistical model calculation was performed after correcting the excitation energies for these losses.

The measured fold distributions of the multiplicity filter were mapped onto the angular momentum space using a Monte Carlo GEANT3 simulation [30]. Here, each fold corresponds to the number of multiplicity detectors fired in an event. The process is described in detail in Ref. [24]. The initial angular momentum distribution of the fusion events required for simulation studies was obtained from the HIPSE calculation. The simulated angular momentum distributions were incorporated in a modified version of the statistical model code CASCADE [31]. The measured high-energy  $\gamma$ -ray spectra were compared with the prediction of the CASCADE code along with a bremsstrahlung component. Within the CASCADE code, the  $\gamma$ -decay rate was calculated by using the principle of detailed balance using a Lorentzian photoabsorption cross section in the inverse channel given by

$$\sigma_{\text{abs}}(E_\gamma) = S_{\text{GDR}} \frac{4\pi e^2 \hbar NZ}{m_p c A} \frac{\Gamma_{\text{GDR}} E_\gamma^2}{(E_\gamma^2 - E_{\text{GDR}}^2)^2 + \Gamma_{\text{GDR}}^2 E_\gamma^2}, \quad (1)$$

where  $E_{\text{GDR}}$ ,  $\Gamma_{\text{GDR}}$ , and  $S_{\text{GDR}}$  are energy, width, and GDR fraction of the total energy weighted dipole sum-rule,  $m_p$  is the proton mass and  $N$ ,  $Z$ , and  $A$  are the neutron, proton, and mass numbers respectively. The  $\gamma$ -ray spectra obtained from the CASCADE code were properly folded with the detector response function, generated using the GEANT3 simulation considering actual experimental conditions. The bremsstrahlung component was parametrized as  $\sigma = \sigma_0 \exp(-E_\gamma/E_0)$ , where the parameters  $\sigma_0$  and  $E_0$  were determined by the visual inspection of experimental  $\gamma$ -ray spectra beyond the statistical component (above  $E_\gamma = 25$  MeV). The estimated values of  $E_0$  for all beam energies were about 8.5 MeV and have large uncertainties due to very poor statistics in this region. We would like to mention here that, similar to the authors of Ref. [19], we also observed that this parametrization has negligible effect on the extracted GDR parameters. Since the GDR parameters are extracted from a statistical model analysis, which depends sensitively

TABLE I. The GDR and other relevant parameters at the specified beam energies. Uncertainties in the inverse level density parameter  $k \approx \pm 0.5$  MeV.

$E_{\text{Lab}}$ (MeV)	$\langle T \rangle$ (MeV)	$S_{\text{GDR}}$	$E_{\text{GDR}}$ (MeV)	$\Gamma_{\text{GDR}}$ (MeV)	$\langle A \rangle$	$\langle Z \rangle$	$k$ (MeV)
116	$2.0^{+0.1}_{-0.1}$	$1.00 \pm 0.02$	$15.0 \pm 0.1$	$7.9 \pm 0.3$	74	36	7.3
140	$2.3^{+0.1}_{-0.2}$	$1.00 \pm 0.03$	$15.8 \pm 0.1$	$10.2 \pm 0.4$	73	35	7.5
160	$2.5^{+0.1}_{-0.2}$	$0.98 \pm 0.03$	$16.2 \pm 0.1$	$11.5 \pm 0.4$	73	35	7.5

on the level density, an accurate knowledge of the NLD is required. For the level density, the Reisdorf [32] prescription as presented in Ref. [33] was used. In this formulation, the level density is mainly governed by the level density parameter given by  $a = \tilde{a}[1 + \frac{\Delta S}{U}\{1 - \exp(-\gamma U)\}]$  [34], where  $\tilde{a} = A/k$ , and  $k$  is called the inverse level density parameter. The value of  $k$  was tuned to match the experimental back-angle neutron spectra (Fig. 1), and the optimum values of  $k$  are shown in Table I. Here  $\Delta S$ ,  $\gamma$ , and  $U$  are the ground state shell correction, shell damping factor, and the intrinsic excitation energy respectively. It should be highlighted that the inverse level density parameter, determined at a given excitation energy by fitting the evaporated neutron spectrum, was used to analyze the high-energy  $\gamma$ -ray spectrum for the extraction of GDR parameters. In Table I, the GDR parameters are shown along with the other relevant quantities, and in Fig. 2 the high-energy  $\gamma$  rays and best-fit results of the statistical

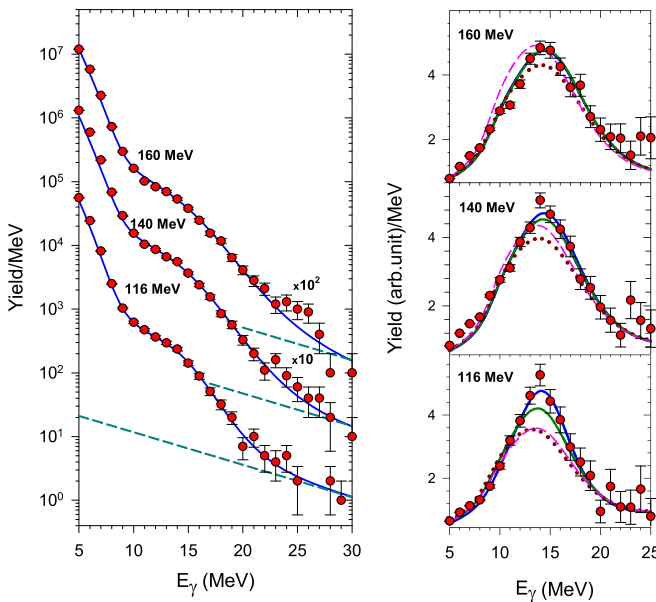


FIG. 2. Measured high-energy  $\gamma$ -ray spectra and divided plots along with best fitted CASCADE calculations (blue continuous lines) at incident energies of 116, 140, and 160 MeV. In the left panel, bremsstrahlung components are shown (cyan dashed line). In the right panel, model calculations based on the fluctuation of nuclear shape are shown. The pink dashed line represents the adiabatic TFSM calculation. The red dotted line and the green solid line correspond to the pTFSM [40] and CTFM [11] calculations, respectively. All the model calculations were performed at  $J = 26\hbar$  (see text).

model calculations are shown along with the corresponding linearized divided plots for average angular momentum  $26\hbar$  ( $\pm 5\hbar$ ) at three different energies. These plots are obtained by dividing both the experimental high-energy  $\gamma$ -ray spectra and the calculated  $\gamma$ -ray spectra (with GDR), by a calculated  $\gamma$ -ray spectra with a constant dipole strength. The GDR parameters were obtained from the best fit to the data (energy interval 8–21 MeV) using a  $\chi^2$ -minimization technique which properly takes into account the sensitivity of the low yield part of an exponential spectrum. A detailed description of this technique can be found in [35]. Uncertainties were estimated from the respective  $\chi^2$  plots according to the procedure given in [36]. It is interesting to note that there is a variation in  $E_{\text{GDR}}$  of about 1.2 MeV. Such variation was also seen in the case of medium mass nucleus  $^{86}\text{Mo}$  and this could be due to a combined effect of high angular momentum and nuclear temperature [37].

The high-energy  $\gamma$  rays are emitted not only from the hot compound in the first steps of its deexcitation but also from the daughter nuclei with decreasing probability. Therefore each  $\gamma$ -ray spectrum is associated with an average temperature and the averaging becomes more and more important as the excitation energy of the compound nucleus increases. The temperature was estimated using the relation  $\langle T \rangle = [(\langle E^* \rangle - \langle E_{\text{rot}} \rangle - E_{\text{GDR}})/a]^{1/2}$  where  $\langle E^* \rangle$  is the average excitation energy (preequilibrium emission corrected) and  $\langle E_{\text{rot}} \rangle$  is the energy bound in the rotation at the average  $J$ . To extract the average temperature in this work, the prescription of Wieland *et al.* [20] was adopted. In this method first a lower cut in excitation energy was determined, below which if we change the GDR width significantly by hand, there will be no effect on the extracted GDR parameters. Then the average values of  $\langle E^* \rangle$ ,  $\langle J \rangle$ ,  $\langle A \rangle$ , and  $\langle Z \rangle$  were calculated when there is 50% of the high-energy  $\gamma$ -ray yield in the GDR region (12–20 MeV), which is emitted within the specified excitation energy interval. The obtained values of the average temperature are 2.0, 2.3, and 2.5 MeV for beam energies 116, 140, and 160 MeV, respectively. A more detailed description of this method and process of error calculation can be found in Ref. [38].

The measured GDR widths for  $^{74}\text{Kr}$  in the present experiment are plotted in Fig. 3 (bottom) as a function of temperature along with the earlier data available at lower excitation energies for  $^{76}\text{Kr}$  [39] ( $\langle J \rangle \approx 9\text{--}17\hbar$ ). The recently measured GDR width for  $^{88}\text{Mo}$  [21] is also shown in Fig. 3 (top) together with the low temperature data for  $^{86}\text{Mo}$  [37],  $^{92}\text{Mo}$  [36], and  $^{100}\text{Mo}$  [36]. It is evident, from this figure, that for  $^{74}\text{Kr}$  the GDR width sharply increases with temperature in the range of  $T = 2\text{--}2.5$  MeV. This is in contradiction to the rather weak dependence of GDR width on temperature in the  $^{88}\text{Mo}$  nucleus, which suggested a saturation of the width. The nice agreement of low temperature data of Mo isotopes with the phenomenological thermal shape fluctuation model (pTFSM) calculation (shown in Fig. 3) proposed by Kusnezov *et al.*, [40] also supports the saturation phenomenon in  $^{88}\text{Mo}$  (for details see Ref. [21]). A part of this “saturation” effect has been thought to be associated with much higher (almost twice) rotational frequency ( $\hbar\omega \approx 1.0$  MeV for  $J \approx 24\hbar$ ) for the same spin in  $^{88}\text{Mo}$  than in  $^{132}\text{Ce}$  [20]. As a



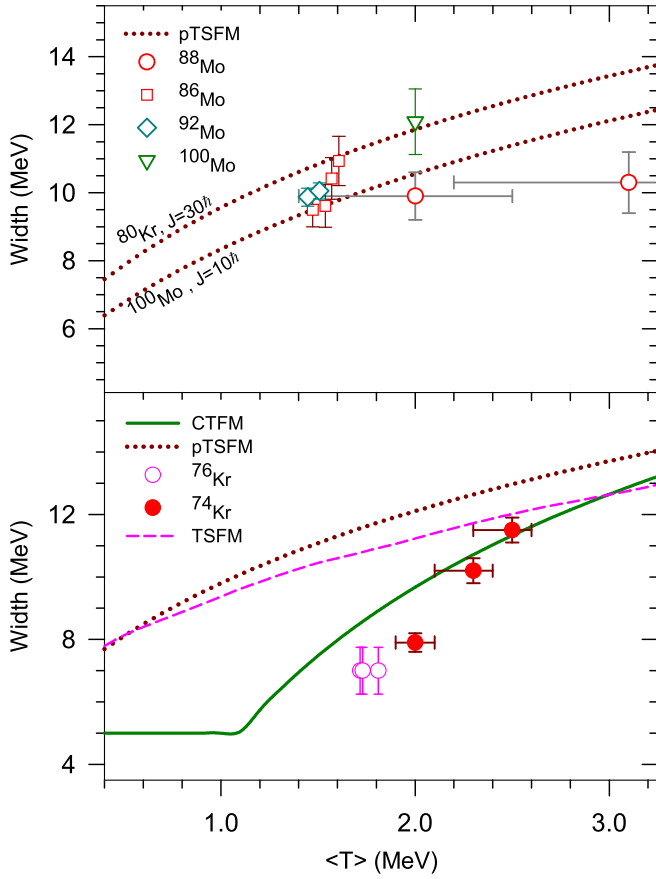


FIG. 3. Plot of GDR width with temperature. Top panel: GDR widths for  $^{88}\text{Mo}$  [21],  $^{86}\text{Mo}$  [37],  $^{92}\text{Mo}$  [36], and  $^{100}\text{Mo}$  [36] along with prediction of pTFSM [40] (see Ref. [21] for details). Bottom panel: The red filled circles are the values for  $^{74}\text{Kr}$  deduced from the present work. Experimental data for  $^{76}\text{Kr}$  [39] (pink open circle) are from previous works. The pink dashed line represents the adiabatic model of TFSM calculation. The red dotted line and the green solid line corresponds to the pTFSM [40] and CTFM [11] calculations, respectively. All the model calculations were performed at  $J = 26\hbar$ .

consequence, the GDR width in  $^{88}\text{Mo}$  at both temperatures is thought to be governed mainly by deformation effects induced by high rotation (splitting of the GDR components) and not so much affected by temperature. However, it is compelling to note that the angular frequency for  $^{74}\text{Kr}$  chosen in this work is even higher ( $\hbar\omega \approx 1.45$  MeV,  $J \approx 26\hbar$ ) and there is no indication of saturation of GDR width in the temperature range of 2–2.5 MeV.

The obtained widths in this work were compared with the models based on the fluctuation of nuclear shape, namely adiabatic TFSM, pTFSM [40], and CTFM [11]. Within TFSM, the GDR strength function at a given  $T$  and  $J$  was calculated as the weighted average of the various line shapes corresponding to different points in the  $\beta$ - $\gamma$  plane; the weight being the Boltzmann factor  $e^{-F(\beta,\gamma)/T}$ , where  $\beta$  and  $\gamma$  are the deformation parameters. The free energy  $F$  was calculated using the Lublin-Strasbourg drop (LSD) model [41] considering only the deformed liquid drop energy (since the shell effect is expected to be dissolved above  $T > 1.5$  MeV). Here,

$E_{\text{GDR}}$  was calculated from the systematics  $18A^{-1/3} + 25A^{-1/6}$  [42], and ground state GDR width  $\Gamma_0$  (at  $T = 0$ ) was taken as 5 MeV (an experimentally known value in nearby nuclei [43]). The temperature-dependent evaporation widths ( $\Gamma_{\text{ev}}$ ) were obtained with the help of statistical model calculation [44,45]. One may observe from Fig. 3 that the results of TFSM calculations (including  $\Gamma_{\text{ev}}$ ) overpredict the measured widths at the temperatures considered in this work. The phenomenological thermal shape fluctuation model (pTFSM) [40] also fails to reproduce the measured widths particularly at low temperatures. Within the critical temperature included thermal shape fluctuation model (CTFM), the GDR width remains constant at the ground state value up to a critical temperature  $T_c = 0.7 + 37.5/A$  due to the GDR induced fluctuation, and it increases thereafter [11]. This model prediction shows reasonable agreement with the measured data. However, the small mismatch at lower temperature may be due to unavailability of proper ground state width. Another possibility could be the presence of any microscopic effect at low temperatures which may shift the  $T_c$  towards higher values (seen earlier also in the case of  $^{201}\text{Tl}$  [11] due to shell effects), which is itself a separate interesting topic to look for using light ion beams. The Lorentzian line shapes predicted by the above models were included within the CASCADE code according to the photoabsorption cross section given in Eq. (1) and compared with the experimental high-energy  $\gamma$ -ray spectra (shown in Fig. 2) after properly folding with the detector's response function.

In summary, an exclusive experimental study of the giant dipole resonance width was performed for  $^{74}\text{Kr}$  in the temperature range of 2–2.5 MeV using the fusion reaction  $^{16}\text{O}$  ( $E_{\text{Lab}} = 116, 140, \text{ and } 160$  MeV) +  $^{58}\text{Ni}$  to search for any saturation of GDR width in medium mass nuclei, which is one of the open issues in this field. The high-energy  $\gamma$  rays and the evaporated neutrons were measured in coincidence with low-energy discrete  $\gamma$ -ray multiplicities. A narrow window of angular momentum distribution around  $26\hbar$  was selected with the help of a  $\gamma$  multiplicity filter array. The nuclear level density parameter, which is an important input for statistical model calculation and for the proper estimation of nuclear temperature, was extracted from the evaporated neutron spectra. From the present study it is observed that there is no indication of saturation of GDR width in  $^{74}\text{Kr}$  at least up to temperature  $T = 2.5$  MeV, even though the associated angular frequency is very high (which was earlier supposed to be one of the reasons behind the saturation effect seen in the case of  $^{88}\text{Mo}$ ). The measured data were compared with the model predictions of TFSM and phenomenological models pTFSM and CTFM, and it is observed that the data are only explained by the prediction of CTFM.

The authors acknowledge Denis Lacroix for providing the updated version of HIPSE code and for his valuable comments and suggestions. The authors would also like to acknowledge A. K. Saha and J. K. Meena for their help during the experimental setup and R. M. Saha for fabricating the  $^{58}\text{Ni}$  target. One of the authors (S. R. Banerjee) acknowledges financial assistance from Science and Engineering Research Board (Government of India) Grant No. CRG-2018-000336.

- [1] M. N. Harakeh and A. van der Woude, *Giant Resonances: Fundamental High-Frequency Mode of Nuclear Excitation* (Clarendon, Oxford, 2001).
- [2] D. Santonocito *et al.*, *Phys. Lett. B* **782**, 427 (2018).
- [3] N. Auerbach and S. Shlomo, *Phys. Rev. Lett.* **103**, 172501 (2009).
- [4] Nguyen Dinh Dang, *Phys. Rev. C* **84**, 034309 (2011).
- [5] D. Mondal *et al.*, *Phys. Rev. Lett.* **118**, 192501 (2017).
- [6] D. R. Chakrabarty *et al.*, *Eur. Phys. J. A* **52**, 143 (2016).
- [7] P. F. Bortignon, A. Bracco, and R. A. Broglia, *Giant Resonances: Nuclear Structure at Finite Temperature* (Harwood Academic, Australia, 1998).
- [8] Y. Alhassid, B. Bush, and S. Levit, *Phys. Rev. Lett.* **61**, 1926 (1988).
- [9] N. D. Dang and A. Arima, *Phys. Rev. Lett.* **80**, 4145 (1998).
- [10] S. Mukhopadhyay *et al.*, *Phys. Lett. B* **709**, 9 (2012).
- [11] D. Pandit *et al.*, *Phys. Lett. B* **713**, 434 (2012).
- [12] B. Dey *et al.*, *Phys. Lett. B* **731**, 92 (2014).
- [13] D. Mondal *et al.*, *Phys. Lett. B* **784**, 423 (2018).
- [14] N. D. Dang and A. Arima, *Phys. Rev. C* **68**, 044303 (2003).
- [15] A. K. Rhine Kumar, P. Arumugam, and N. D. Dang, *Phys. Rev. C* **91**, 044305 (2015).
- [16] A. Bracco *et al.*, *Phys. Rev. Lett.* **62**, 2080 (1989).
- [17] G. Enders *et al.*, *Phys. Rev. Lett.* **69**, 249 (1992).
- [18] H. J. Hofmann *et al.*, *Nucl. Phys. A* **571**, 301 (1994).
- [19] M. P. Kelly, K. A. Snover, J. P. S. van Schagen, M. Kicinska-Habior, and Z. Trznadel, *Phys. Rev. Lett.* **82**, 3404 (1999).
- [20] O. Wieland *et al.*, *Phys. Rev. Lett.* **97**, 012501 (2006).
- [21] M. Ciemala *et al.*, *Phys. Rev. C* **91**, 054313 (2015).
- [22] A. K. Rhine Kumar, P. Arumugam, N. D. Dang, and I. Mazumdar, *Phys. Rev. C* **96**, 024322 (2017).
- [23] S. Mukhopadhyay *et al.*, *Nucl. Instrum. Methods A* **582**, 603 (2007).
- [24] D. Pandit *et al.*, *Nucl. Instrum. Methods A* **624**, 148 (2010).
- [25] G. Dietze and H. Klein, Physikalisch-Technische Bundesanstalt Report No. PTB-ND-22, 1982 (unpublished).
- [26] P. Roy *et al.*, *Nucl. Instrum. Methods A* **901**, 198 (2018).
- [27] V. L. Kravchuk *et al.*, *EPJ Web Conf.* **2**, 10006 (2010).
- [28] A. Giaz *et al.*, *Phys. Rev. C* **90**, 014609 (2014).
- [29] D. Lacroix, A. Van Lauwe, and D. Durand, *Phys. Rev. C* **69**, 054604 (2004).
- [30] R. Brun *et al.*, GEANT3, CERN Report No. CERN-DD/EE/84-1, 1986 (unpublished).
- [31] F. Pühlhofer, *Nucl. Phys.* **280**, 267 (1977).
- [32] W. Reisdorf, *Z. Phys. A* **300**, 227 (1981).
- [33] M. Kicinska-Habior, K. A. Snover, C. A. Gossett, J. A. Behr, G. Feldman, H. K. Glatzel, J. H. Gundlach, and E. F. Garman, *Phys. Rev. C* **36**, 612 (1987).
- [34] A. V. Ignatyuk, G. N. Smirenkin, and A. S. Tishin, *Yad. Fiz.* **21**, 485 (1975) [*Sov. J. Nucl. Phys.* **21**, 255 (1975)].
- [35] S. Ceruti *et al.*, *Phys. Rev. C* **95**, 014312 (2017).
- [36] M. Kicinska-Habior, K. A. Snover, J. A. Behr, C. A. Gossett, J. H. Gundlach, and G. Feldman, *Phys. Rev. C* **45**, 569 (1992).
- [37] S. K. Rathi, D. R. Chakrabarty, V. M. Datar, S. Kumar, E. T. Mirgule, A. Mitra, V. Nanal, and H. H. Oza, *Phys. Rev. C* **67**, 024603 (2003).
- [38] A. Bracco *et al.*, *Mod. Phys. Lett. A* **22**, 2479 (2007).
- [39] E. F. Garman, K. A. Snover, S. H. Chew, S. K. B. Hesmondhalgh, W. N. Catford, and P. M. Walker, *Phys. Rev. C* **28**, 2554(R) (1983).
- [40] D. Kusnezov, Y. Alhassid, and K. A. Snover, *Phys. Rev. Lett.* **81**, 542 (1998), and references therein.
- [41] K. Pomorski and J. Dudek, *Phys. Rev. C* **67**, 044316 (2003).
- [42] J. J. Gaardhøje *et al.*, *Annu. Rev. Nucl. Part. Sci.* **42**, 483 (1992).
- [43] A. V. Varlamov *et al.*, *Atlas of Giant Dipole Resonances*, INDC(NDS)-394 (IAEA, Vienna, 1999).
- [44] V. Weisskopf, *Phys. Rev.* **52**, 295 (1937).
- [45] P. Frobrich and I. I. Gontchar, *Phys. Rep.* **292**, 131 (1998).